

Wind-Forced Upwelling: The Role of the Surface Mixed Layer

JOHN F. MIDDLETON

School of Mathematics, University of New South Wales, Sydney, New South Wales, Australia

(Manuscript received 1 June 1998, in final form 19 November 1998)

ABSTRACT

A numerical study is made of the dynamics of the circulation that arises from forcing by a steady, uniform alongshore wind over a uniform zonal shelf in the Southern Hemisphere. The results show that most of the upwelling is confined to the region inshore of the shelf break. Over the slope and within the region of wind forcing the circulation is found to be dominated by the growth of both an anticyclonic and a cyclonic eddy, an offshore flow, and downwelling.

Two new mechanisms are identified as being responsible for these features of the upwelling circulation. First, the offshore advection of alongshore momentum ($\rho_0 u v_x$) within the surface mixed layer (SML) is shown to accelerate the alongshore current near the eastern end of the region of wind forcing, leading to a sharpening of the cross-shelf gradient of sea level and an excess in the alongshore transport. This excess transport acts to raise sea level, leads to downwelling below the base of the SML, and causes the growth of the anticyclonic eddy. A scaling suggests that the advective term $\rho_0 u v_x$ will be important provided that $u_* L_w (N/f)^{1/2} / (f L_x^2)$ is of order one or larger. Here, u_* , f , N , L_w , and L_x denote the surface friction velocity, Coriolis parameter, buoyancy frequency, fetch of wind forcing, and a scale for the shelf width. The magnitude of the advective term increases with near-surface stratification, since the SML depth will be smaller and the cross-shelf velocity u larger, and wind fetch and decreasing shelf width, since the alongshore shelf velocity v will be larger.

A second important effect is argued to result from the geostrophic cross-shelf flow associated with the alongshore gradients of density within the SML. The cross-shelf flows, largest near the edges of the region of wind forcing, act to raise (lower) sea level leading to an additional onshore (offshore) flow, vorticity production, and growth of the eddies.

1. Introduction

Wind-forced upwelling along continental shelves has been the subject of numerous investigations (Brink 1983; Smith 1994). Major experimental programs have been conducted along the western shelves of the United States, Spain, and Peru (Mooers et al. 1976; Huyer et al. 1987). These and other studies have demonstrated that upwelling is a fully three-dimensional process involving the dynamics of fronts, the surface and bottom boundary layers, baroclinic instability and filament formation, undercurrents, and the effects of variations in shelf and coastline. Models for upwelling have tended to focus on some subset of the above dynamics and have progressed from semianalytic solutions for undercurrents (McCreary 1981) to numerical studies of filament formation (Haidvogel et al. 1991).

Most recently, Allen et al. (1995) returned to a two-dimensional, high-resolution model of upwelling where alongshore variations were precluded. The study fo-

cused on the nearshore zone and the upwelled front was shown to be subject to both up- and downwelling with a two-day period and reminiscent of the two-cell circulation model formulated by Mooers et al. (1976) using hydrographic and moored current meter data. Of particular relevance here was the identification of the bottom boundary layer as a major conduit for onshore transport as the circulation asymptotes towards a steady state. Results presented by Allen et al. (1995) show that, as the steady state is approached, the transport within the bottom boundary layer, inshore of the shelfbreak, becomes as large as that within the surface Ekman layer. Over the steep slope, the boundary layer transport is smaller. The resultant cross-shelf divergence acts to draw water down into the bottom boundary layer near the shelf break. The downwelling here can extend into the thermocline although it is necessarily localized to the region of the shelf break since, shoreward of this region, most of the onshore transport is carried within the thin bottom boundary layer.

The logical extension of this two-dimensional study involves upwelling driven by a wind of finite alongshore fetch and over a topographically uniform shelf. Surprisingly, the only primitive equation studies that have been made under these conditions are those by Sugi-

Corresponding author address: Dr. John F. Middleton, School of Mathematics, University of New South Wales, Sydney 2052, Australia.
E-mail: john.middleton@unsw.edu.au

nohara (1982) and Suginothara and Kitamura (1984). Suginothara (1982) examined the short term (0–14 day) evolution of an upwelling-favorable current system and found that a weak undercurrent developed below the equatorward coastal jet for an eastern boundary regime. The setup of the current system was found to be qualitatively described by the passage of the first two coastal-trapped waves (CTWs). A similar result was found by Wang (1982) and, for the short-term circulation driven by downwelling-favorable winds (Middleton and Cirano 1999).

Suginothara and Kitamura (1984) considered the long time (0–160 days) evolution of the current system and, for an f -plane, found that the weak undercurrent ultimately disappeared. Surprisingly, the inclusion of bottom friction did not lead to any substantial change in the results, suggesting that the bottom boundary layer plays only a minor role in the overall dynamics. In addition, the authors describe the development of an anticyclonic eddy in the region of wind forcing and near the shelf edge. By day 160, the near surface poleward speed of the eddy was about 5 cm s^{-1} , while that of the equatorward coastal jet was about 20 cm s^{-1} . In geostrophic and hydrostatic balance, the existence of such an eddy would require that sea level had been raised over the shelf edge, while isopycnals within the thermocline had been downwelled. The authors state that the eddy results from a two-cell circulation (Suginothara 1977) and otherwise claim that “the whole stage response is accounted for by CTW dynamics.” An explanation of the nature and cause of this anticyclonic eddy is a major objective of this study. To this end, the shelf topography used here is similar to that adopted by these authors (and Suginothara 1982), where the 150-m isobath lies approximately 35 km from the coast. The stratification assumed here is also similar, although the offshore internal deformation radius of 10 km is about half of the 24 km obtained by Suginothara and Kitamura (1984) since the Coriolis parameter they assumed ($5 \times 10^{-5} \text{ s}^{-1}$) is half that used below.

In particular, consideration is given below to the role of the surface mixed layer (SML) in determining the circulation over the shelf and slope and the nature and cause of the anticyclonic eddy. Two new mechanisms are identified as being responsible for the anticyclonic eddy and associated offshore transport and downwelling. Results for an f plane will only be presented since this study is motivated in part by a desire to understand upwelling along the zonally oriented shelves of the Great Australian Bight (Schahinger 1987). The effects of Rossby wave dispersion are discussed elsewhere (Suginothara and Kitamura 1984; Middleton and Cirano 1999).

In section 2, an outline is given of the boundary conditions and configuration of the Princeton Ocean Model (Blumberg and Mellor 1987). In section 3, an overview of the circulation is presented, while in section 4 the cause of the anticyclonic eddy and downwelling is de-

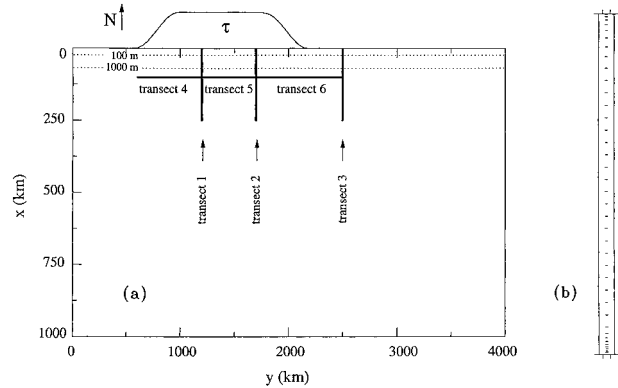


FIG. 1. (a) The model domain including the transects for analysis and the 100- and 1000-m depth contours (dotted) of the zonal shelf. The direction north (N) and region of wind forcing are indicated above the panel. The seaward ocean has a uniform depth of 1000 m. (b) The vertical distribution of the 40 sigma levels.

termined. To this end, a model for the geostrophic adjustment of an “upwelled” density anomaly is presented in the appendix. In section 5 a brief discussion of the results obtained far from the region of wind forcing is made, and in section 6 a summary is presented.

2. Model configuration

The numerical model used is the 1992 version of the Princeton Ocean Model, configured for the domain shown in Fig. 1. We take x to be the offshore coordinate and y to be the alongshore coordinate. The shelf will be taken to extend from west to east as indicated since we are interested in upwelling over zonal shelves.

The shelf depth $h(x)$ is uniform in the alongshore direction and the top 350 m is illustrated in Fig. 3. The shelf intercepts the deep ocean at $(x, h) = (60 \text{ km}, 1000 \text{ m})$ (Fig. 1). For convenience, we will define the shelf break to coincide with the 150-m isobath ($x \approx 35 \text{ km}$). In the following, regions inshore and offshore of the shelf break will be referred to as the shelf and slope, respectively. The x -grid size varies from about 2 km over the shelf and slope to 8 km at the intercept with the deep ocean. Beyond this point, the grid size increases linearly by 20% to a maximum of 82 km at the southern end of the ocean basin ($x = 1017 \text{ km}$). The y -grid size decreases from 40 km at the western end of the domain to 20 km at $y = 500 \text{ km}$. For $y \in [500, 2500] \text{ km}$, the grid size is fixed at 20 km, while farther to the east the grid size increases linearly to 60 km, yielding an alongshore extent of 4000 km. A total of 45 and 145 cells are used in the x and y directions, while in the vertical 40 sigma levels are adopted with greatest resolution near the surface and bottom (Fig. 1). To satisfy the CFL criteria, the internal and external time steps are chosen to be 400 and 10 seconds, respectively.

The horizontal eddy viscosity (and diffusivity) and

the bottom drag coefficient are taken to be $50 \text{ m}^2 \text{ s}^{-1}$ and $C_D = 2.5 \times 10^{-3}$, respectively, and a Coriolis parameter for the Southern Hemisphere is chosen as $f = -10^{-4} \text{ s}^{-1}$. The vertical diffusivities of momentum, salt, and heat are determined from the Mellor–Yamada turbulence closure scheme and are thus generally zero in the interior where the velocity shear is small.

The boundary conditions are similar to those adopted by McCreary et al. (1991). No energy should be present at the western boundary since, in the Southern Hemisphere, CTWs can only propagate with the coast on the left. However, model results show that some energy does propagate to the west (along the southern open boundary), so an Orlanski radiation condition was adopted for the western boundary. To absorb any residual energy near the western boundary, a Rayleigh sponge was adopted for sea level (η), the depth-averaged velocities (U , V) and the depth-dependent velocities (u , v). For the sponge, the damping coefficient increases linearly from zero at $y = 433 \text{ km}$ to a value of $1/(2400 \text{ s})$ at the western boundary ($y = 0$).

A modified Orlanski condition was applied to all variables at the southern open boundary since use of an Orlanski condition led to large numerical instabilities after a few days of model evolution (McCreary et al. 1991). At the eastern boundary a zero gradient condition was applied so as to allow for the inflow of the westward coastal jet.

Forcing of the model was accomplished by an alongshore wind stress, tapered in the alongshore direction from zero to a constant value of $\tau = 0.1 \text{ Pa}$ between $y = 1000 \text{ km}$ and $y = 1800 \text{ km}$ (Fig. 1). The net surface Ekman flux is 1.2 Sv ($\text{Sv} \equiv 10^6 \text{ m}^3 \text{ s}^{-1}$) indicating an effective fetch of $L_w = 1200 \text{ km}$.

The surface and bottom fluxes of heat and salt are set to zero or determined in the following way. The surface flux of heat is denoted by $W_s \Delta T$ where ΔT is the difference between the surface temperature at time t and time zero and W_s a scale for the vertical velocity. The latter is chosen so as to minimize the SML density gradients. In particular, with $HU_E = \tau/(f\rho_0)$ the surface Ekman flux, ρ_0 an average density, and L_m an offshore length scale, the vertical flux and W_s are chosen such that deficit of heat advected offshore by the SML is lost vertically through the surface within $L_m = 20 \text{ km}$ of the coast: $HU_E \Delta T = W_s L_m \Delta T$. The scale $W_s = HU_E/L_m = 5 \times 10^{-5} \text{ m s}^{-1}$ results, and a similar flux is used for salt.

The model solutions were found to be subject to two-grid point instabilities that were most evident in the alongshore direction. Since the alongshore scale of the uncontaminated solutions should exceed the $3\Delta y$ scale of 60 km , the instabilities were kept under reasonable control by applying a Shapiro filter in the alongshore direction and to all time-dependent variables. For sea level the filter may be written as $\eta_{i,j} = (1 - \gamma)\eta_{i,j} + 0.5\gamma[\eta_{i,j-1} + \eta_{i,j+1}]$, where once a model run day, γ was fixed at 0.5 so as to provide a severe filter. At all other

time steps γ was fixed at 0.1 . The model results were also filtered in time so as to eliminate inertial waves.

As a check on artificial pressure gradients that arise from the sigma coordinate system, the model was run for 30 days without any wind forcing. As desired, the velocity field was near zero, with a maximum value of 0.5 cm s^{-1} over the outer slope (depth 300 m). Additional tests were made by doubling the alongshore or offshore extent of the model domain. Almost no change was found in the solutions, indicating that the results are insensitive to the eastern and offshore boundary conditions.

3. An overview of the circulation: The central experiment

Here upwelling solutions are obtained with the surface fluxes of heat and salt set to zero and the component of wind stress set equal to 0.1 Pa . Both an anticyclonic and cyclonic eddy develop within the forcing region, and the associated cross-shelf flow and downwelling dominate the circulation over the shelf slope. In the following, reference will be made to a westward coastal jet (eastward undercurrent), defined to be that which moves in the same (opposite) direction as the wind.

To begin, consider the results at day 10, which show that the offshore Ekman transport depresses sealevel by up to 14 cm at the coast (Fig. 2a). A feature of the solutions is the presence of a high pressure ridge located near the edge of the shelf ($x \approx 50 \text{ km}$), which is attributed to the vortex squashing that results as fluid columns over the shelf are drawn onshore (Suginohara 1977). A similar result was found by Suginohara and Kitamura (1984). With the exception of the nearsurface eastward flow associated with the high, the flow over the shelf at transect 2 is everywhere to the west and the isopycnals are upwelled toward the coast (Figs. 3a,b). The circulation here is generally consistent with that predicted by a linear CTW model (Suginohara 1982).

Now consider the results at day 60. The ridge of high pressure has developed into a well-defined anticyclonic eddy at the eastern end of the forcing region (Fig. 2b). To the west, the high pressure ridge has been replaced by a pressure trough that extends more than 160 km from the coast. The alongshore velocity field at transect 2 and day 60 is shown in Fig. 3c and is qualitatively similar to that at day 10. An eastward undercurrent is not found over the slope, but a weak eastward flow is found near the surface and near the edge of the shelf. This eastward current is associated with the eddy shown in Fig. 2b.

While the results here are similar to those reported by Suginohara and Kitamura (1984), they do differ from that obtained from linear CTW theory (Suginohara 1982) and from that found where alongshore variations are excluded (Allen et al. 1995). As will be shown (section 4), the seemingly odd results above arise from the

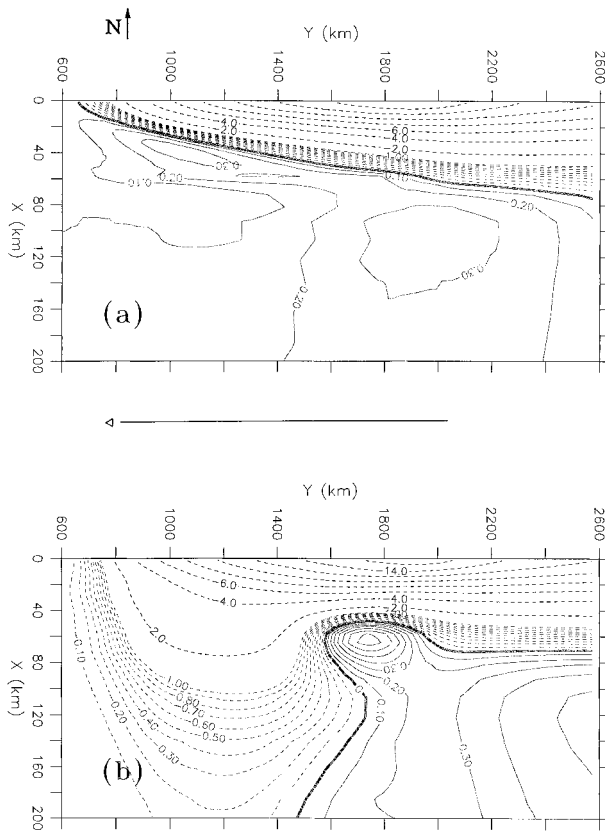


FIG. 2. Central experiments results. (a) The sea level field at day 10. The contour interval is 2 cm for $\eta \leq -1$ cm and 0.1 cm for $\eta \geq -1$ cm. Dashed contours indicate negative sea level displacement. The direction north (N) is indicated above the panel. The region of wind forcing is indicated below the panel by the arrow and the edge of the shelf is located at $x = 60$ km. (b) As in (a) but at day 60.

effects of nonlinear advection and gradients of density within the SML.

Returning to the results at day 60, those for density (Fig. 3d) indicate that most of the upwelling is confined to depths of less than 200 m and within 40 km of the coast. The cross-shelf velocity (u , $100w$) at days 10 and 60 is presented in Figs. 3e and 3f, and for clarity, results are excluded for the SML in the top 50 m of the water column. The cross-shelf velocity field shown does indicate that, beyond the shelf break ($x \approx 35$ km), water is drawn downward toward the shelf and slope, and that this downwelling extends from the base of the SML to depths of over 500 m. The initial depth of the $26.6\sigma_t$ contour is shown in Fig. 3d, and the downwelling acts

to depress the isopycnals within the thermocline and below the center of the anticyclonic eddy.

There is no strong evidence to suggest that the downwelling found here is related to the development of a two-cell circulation due to the density gradients within the SML. For a two-cell circulation, the downwelling takes place on the inshore side of the SML front and is accompanied by upwelling on the offshore side of the front (Suginohara 1977). The downwelling shown in Fig. 3 occurs both in the nearshore zone, where the SML gradient ρ_x is largest, but also over and beyond the shelf break where the gradient is much smaller. The offshore upwelling expected for a two-cell circulation is not found.

To gauge the relative importance of density gradients within the SML, we examine terms in the momentum equations integrated over the depth of the water column. In particular with g , the acceleration due to gravity, and the pressure due to density (ρ), denoted by

$$p' = g \int_z^0 \rho dz, \quad (1)$$

the depth-integrated momentum equation may be written as

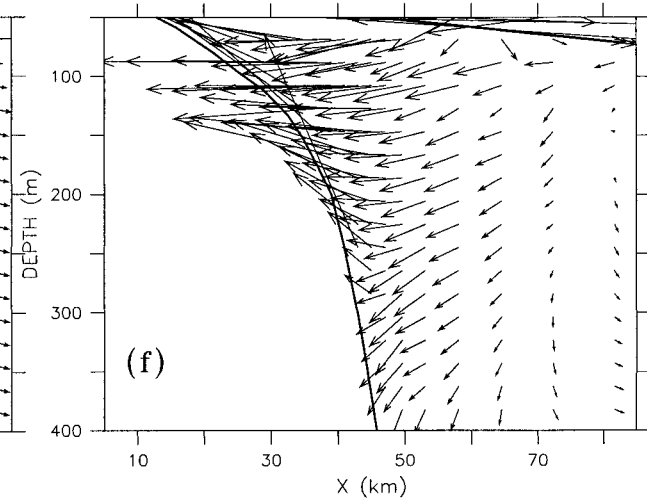
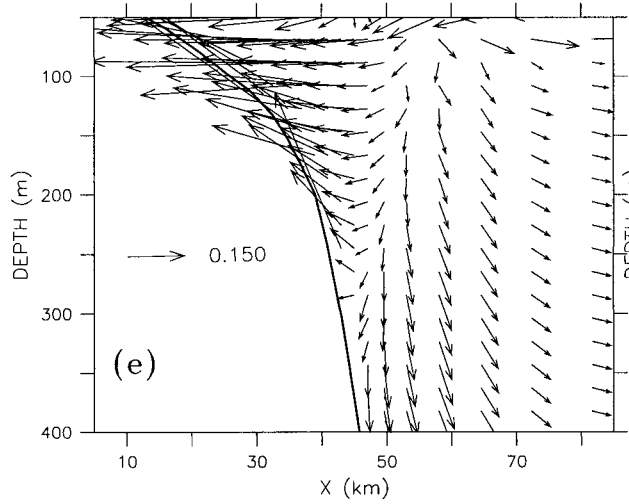
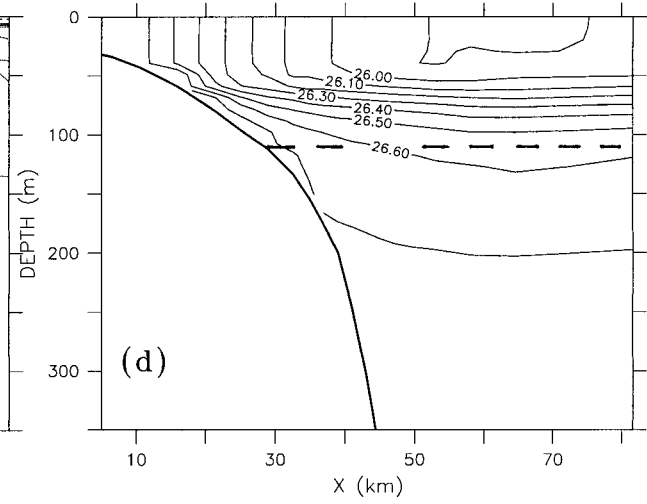
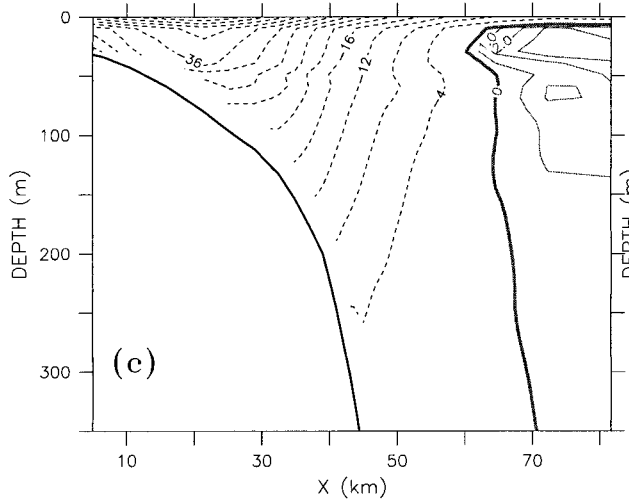
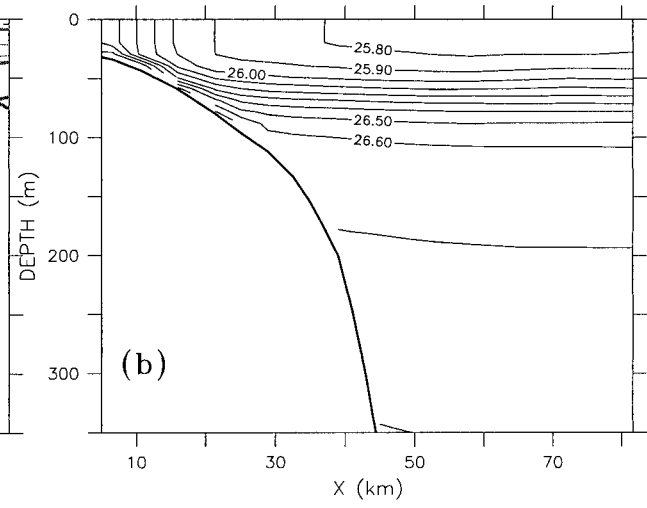
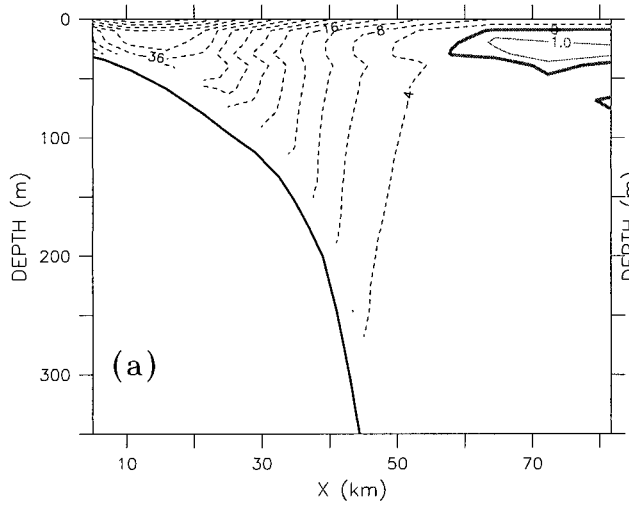
$$\rho_0 h \partial U / \partial t = \underbrace{\rho_0 f h V}_{CFX} - \underbrace{\rho_0 g h \eta_x}_{SGX} - \underbrace{h P_x}_{DGX} \quad \text{and} \quad (2a)$$

$$\rho_0 h \partial V / \partial t = -\underbrace{\rho_0 f h U_r}_{CFY} - \underbrace{\rho_0 g h \eta_y}_{SGY} - \underbrace{h P_y}_{DGY} - \underbrace{\tau^b}_{BSY}, \quad (2b)$$

where the depth-average of (u , v) and p'_x , p'_y are denoted by (U , V) and P_x , P_y , respectively. The bottom friction term in (2a) has been deleted since it was always found to be negligible. Nonlinear and horizontal diffusion terms are also neglected. The labels used for each momentum term in the plots are indicated above. Note also that, in (2b) and in the plots, the alongshore wind stress τ has been subtracted from the Coriolis term and results for the residual $CFY = \rho_0 f h U_r$ are presented: the residual transport hU_r is defined as the total cross-shelf transport less the surface Ekman transport due to the wind. Estimates of the horizontal density gradients that arise within the SML are also presented. Since pressure is continuous with depth, the forces that arise due to gradients within the SML, depth 40 m, extend over the entire water column and will be denoted by (DGX_s , DGY_s). With an implied change of sign, the forces SGX , DGX , etc. will also be referred to as gradients of sea level and density.

Terms in the cross-shelf momentum equation for day

FIG. 3. Central experiment results. (a) The alongshore velocity field v at transect 2 and day 10. The solid (dashed) contours indicate flow to the east (west). Units cm s^{-1} . Note that the contour interval is 4 cm s^{-1} (1 cm s^{-1}) for flow to the west (east). (b) The density field σ_t at transect 2 and at day 10. Units kg m^{-3} , interval 0.1 kg m^{-3} . (c) As in (a) but for day 60. (d) As in (b) but for day 60. The horizontal dashed line indicates the initial position of the $26.6\sigma_t$ contour. (e) The (u , $100w$) vector field at transect 2 and day 10. A vector of length 0.15 cm s^{-1} vector is indicated. Note that for clarity, results for the SML in the top 50 m have been excluded from the plot. (f) As in (e) but for day 60.



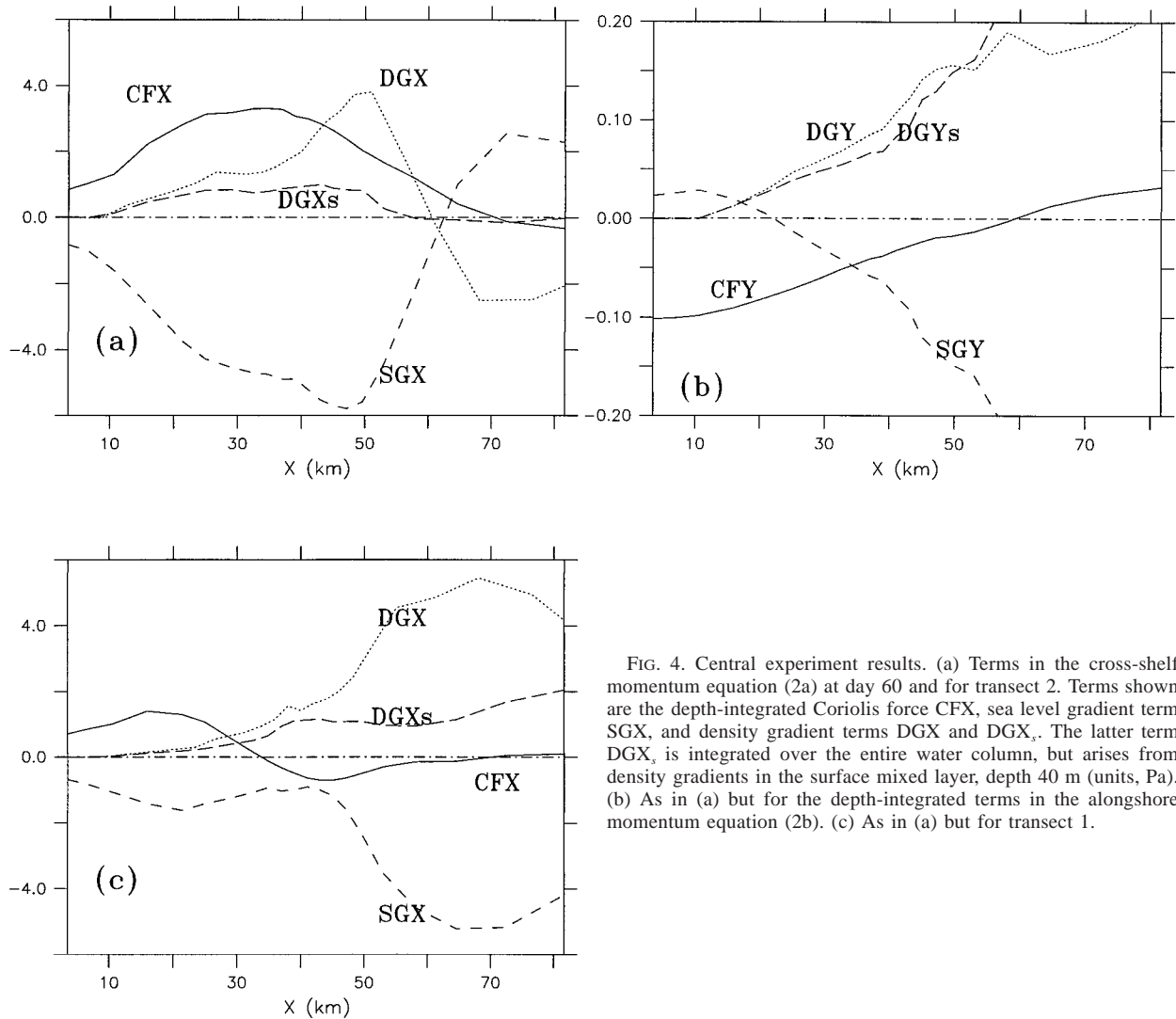


FIG. 4. Central experiment results. (a) Terms in the cross-shelf momentum equation (2a) at day 60 and for transect 2. Terms shown are the depth-integrated Coriolis force CFX, sea level gradient term SGX, and density gradient terms DGX and DGX_s. The latter term DGX_s is integrated over the entire water column, but arises from density gradients in the surface mixed layer, depth 40 m (units, Pa). (b) As in (a) but for the depth-integrated terms in the alongshore momentum equation (2b). (c) As in (a) but for transect 1.

60 and transect 2 are presented in Fig. 4a. As shown, the cross-shelf force due to sea level SGX is largest over the continental slope due to the high associated with the eddy. Beyond the center of the eddy ($x \approx 60$ km), the force SGX changes sign and becomes positive. Shoreward of the center of the eddy, DGX is positive and directed offshore due to the upwelling of dense water. The contribution DGX_s made by the SML is also large and around half of the total over the continental slope at $x = 40$ km. Farther offshore, DGX also changes sign due to the downwelling and eddy formation.

The results for the alongshore pressure gradient at transect 2 (Fig. 4b) also highlight the importance of the SML. As shown, the contribution DGY_s made by the SML dominates the total and is positive and directed to the east due to the upwelling and offshore advection of dense water. Since the SML gradient dominates the total, the alongshore pressure force will vary little with depth and acts to drive a depth-independent onshore geo-

strophic velocity below the SML. The velocity u over the continental slope (Fig. 3f) is not inconsistent with such forcing, being both onshore and approximately independent of depth. As will be shown, the alongshore density gradient is important in determining the details of the eddy patterns found over the slope.

Results are also presented for transect 1, which lies near the western end of the forcing region and within the cyclonic eddy. The cross-shelf gradient of sea level over the slope (Fig. 4c) is much smaller than at transect 2 and the opposing thermal-wind shear that arises predominantly from the SML is sufficient to drive an eastward undercurrent of up to 4 cm s^{-1} (Fig. 5a). The cross-shelf flow over the slope is directed offshore and is downwelling favorable (Fig. 5c). Results obtained 50 km from the coast (Fig. 5d) show that the offshore flow that is driven by the anticyclonic and cyclonic eddies extends over much of the forcing region.

Further insight into the circulation may be gleaned

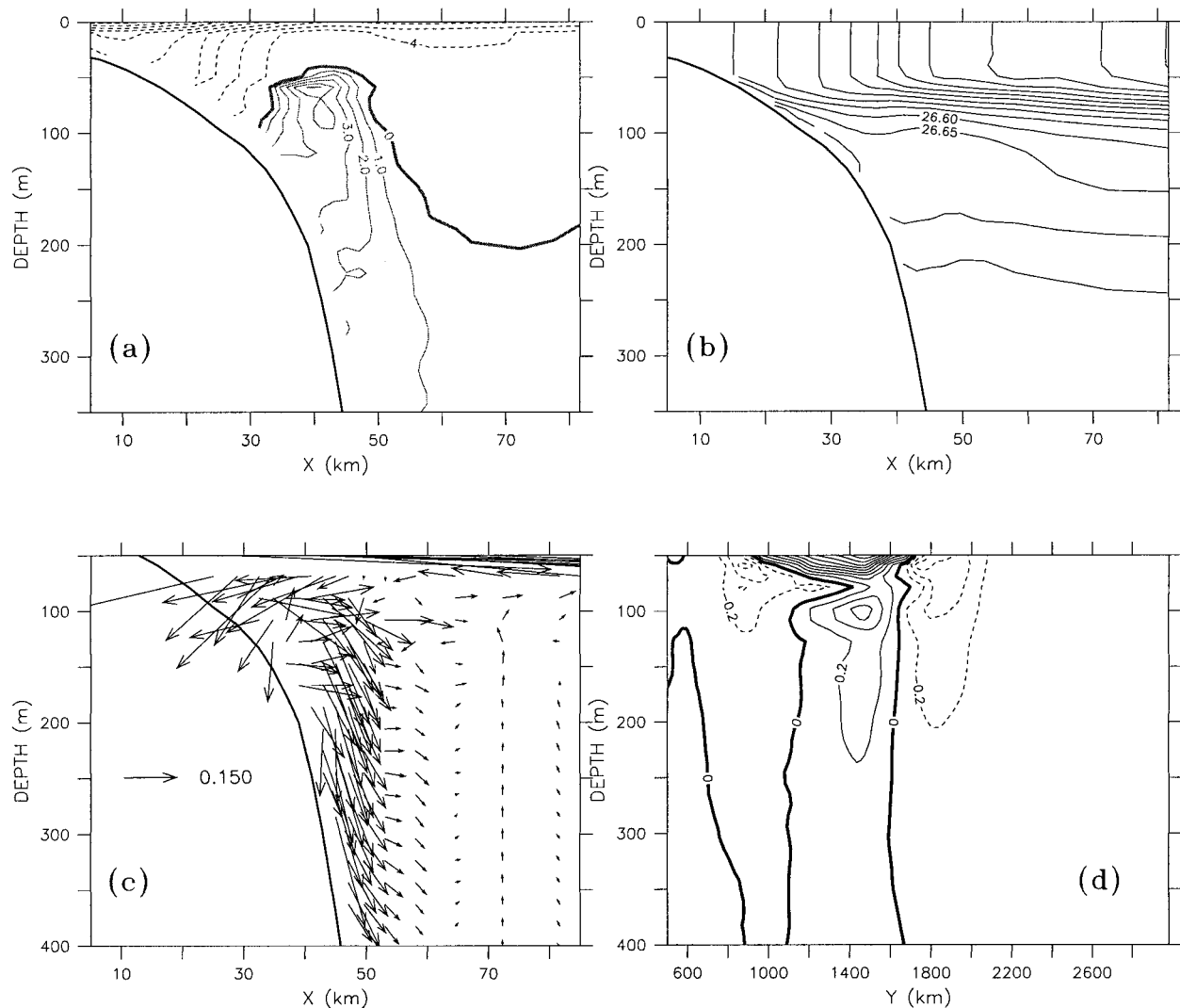


FIG. 5. Central experiment results at transect 1 and day 60. (a) The alongshore velocity field v . The solid (dashed) contours indicate flow to the east (west) with an interval of 4 cm s^{-1} (1 cm s^{-1}). (b) The density field σ_r . Units kg m^{-3} , contour interval 0.1 kg m^{-3} . (c) The $(u, 100w)$ vector field. A vector of length 0.15 cm s^{-1} vector is indicated. Note that for clarity, the SML results in the top 50 m have been excluded from the plot. (d) The cross-shelf velocity u obtained 50 km from the coast at day 60. The contour interval is 0.2 cm s^{-1} . Note that for clarity, the SML results in the top 50 m have been excluded from the plot.

from the net transports presented in the schematic (Fig. 6a). At the top of the schematic, the surface Ekman transports are shown while the horizontal arrows indicate the transports (integrated from the coast to $x = 100 \text{ km}$) associated with the westward coastal jet and eastward undercurrent. The arrows at the bottom of the schematic indicate the *net* transport through transects 4, 5, and 6. As shown, the transport of the eastward undercurrent is relatively small compared to that of the westward coastal jet and the total drawn offshore by the wind (1.2 Sv). At transect 2, the transport of the eastward undercurrent is due entirely to the eastward (near-surface) flow of the eddy.

However, the most notable results concern the alongshore transport of the westward coastal jet through tran-

sects 2 and 3. In the absence of any offshore flow below the SML, the transport through transect 2 should be about 0.9 Sv so as to balance that which is drawn through transect 1 (0.45 Sv) and offshore by the wind (0.5 Sv). Instead, the transport of the westward coastal jet is 1.4 Sv and 50% larger than this value. The excess must go elsewhere and, as shown in Fig. 6a, is largely accounted for by the 0.5 Sv that is directed through the offshore transect 5 by the eddies shown in Fig. 2. In the following it will be shown that this excess in transport, and the eddy growth and downwelling, are strongly dependent on the dynamics of the SML within the region of wind forcing.

It will turn out, however, that the circulation at transect 3 (300 km to the east of the region of wind forcing)

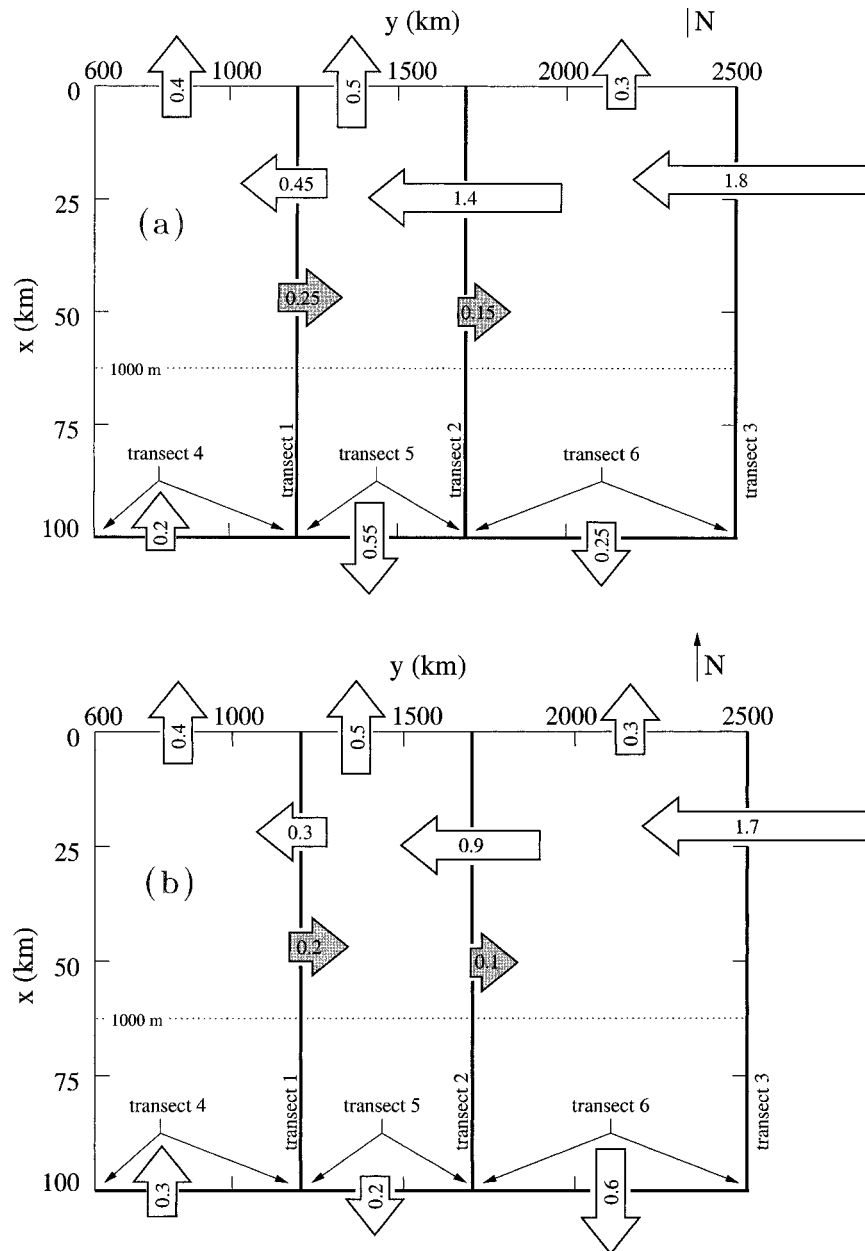


FIG. 6. Net transports. A schematic of the net transports (units Sv) through transects 1 to 6 at day 60. The direction north (N) is indicated above the panel. The eastward and westward directed arrows indicate the transport associated with the westward coastal jet and eastward undercurrent (shaded). The offshore transports are indicated at the bottom of the panel. The transports indicated at the coast (top of the panel) correspond to the offshore flow driven by the wind-forced Ekman transport. (a) Central experiment results at day 60. (b) Linear experiment results at day 60.

is only weakly dependent on the effects of the SML. From Fig. 6a, the alongshore transport through transect 3 is about 1.8 Sv and 50% larger than the 1.2 Sv that drawn offshore by the wind. It might be presumed that the excess here is simply a response to the SML effects and the transport within the forcing region. Coastal-trapped waves propagate information away from the region of forcing and towards transect 3. Surprisingly, the

dynamics and transport at transect 3 are only weakly related to SML effects and further discussion of the far-field results is deferred until section 5.

4. The cause of the eddies and downwelling

As noted, the growth of the eddies and downwelling over the slope do not seem to be related to a two-cell

circulation since this would occur closer inshore where the cross-shelf density gradients are largest. Rather, two new mechanisms for the formation of the eddies are identified. The most important involves the cross-shelf advection of alongshore momentum $\rho_0 uv_x$ within the SML, which acts to accelerate the flow and leads to the excess transport and convergence within the region of wind forcing. The second mechanism is argued to involve the alongshore gradients of density that, through geostrophy, can drive cross-shelf flows leading to vortex stretching and squashing.

A third mechanism for downwelling involves the cross-shelf divergence of the flow within the bottom boundary layer (Allen et al. 1995). Such downwelling should be confined to the shelfbreak region and therefore is not of great importance to the eddy formation and convergence described above.

As a check on this, the model was first rerun with the nonlinear terms retained but with the bottom drag coefficient set to zero. In this case a bottom boundary layer is precluded, and an anticyclonic eddy and downwelling throughout the thermocline were again found. Alongshore velocities up to 1 m s^{-1} were obtained in these solutions and the amplitude of the anticyclonic eddy was about 10 cm, or an order of magnitude larger than that shown in Fig. 2. The larger eddy amplitude is consistent with the hypothesis that the convergence and downwelling are caused by the nonlinear term $\rho_0 uv_x$ since v_x is larger in the case of zero bottom friction.

a. Nonlinear effects

To examine the importance of the nonlinear effects, the magnitude of the advective terms was examined, and by far the largest term found was that for the cross-shelf advection of alongshore momentum $-\rho_0 uv_x$. Representative values of this term, $-\rho_0 uv_y$ and $-\rho_0 wv_z$, are illustrated in Fig. 7a and the magnitude of $\rho_0 uv_x$ is largest within the SML (depth $H_m = 40 \text{ m}$), due to the larger offshore Ekman velocity. Near the surface, the term $\rho_0 uv_x$ does not change greatly between days 10 and 60 and thus may be important to the downwelling found over these times (Figs. 3e,f). Indeed, as shown in Fig. 7b, the average $-\rho_0 \overline{uv_x}$ (taken over H_m), is comparable to the forces, $-\rho_0 g \eta_y$ and $-\overline{p_y}$, that arise from sea level and density variations within the SML. Over 10 days, the maximum value of the term $-\rho_0 \overline{uv_x}$ shown in Fig. 7b is large enough to accelerate the alongshore velocity by about 0.5 m s^{-1} .

Now consider the results in Fig. 8 for sea level and the average $-\rho_0 \overline{uv_x}$. The magnitude of the latter is largest near the eastern end of the forcing region. Outside of the forcing region $-\rho_0 \overline{uv_x}$ is smaller since the surface Ekman velocity vanishes. Within the SML, the sign of this advective term is such as to accelerate the alongshore velocity and increase the westward transport above that which is drawn offshore by the surface Ekman flux. This acceleration and increase in transport

occurs near the eastern end of the forcing region and should lead to the anticyclonic eddy, sea level ridge, and downwelling illustrated in Figs. 2 and 3.

Indeed, when $\rho_0 uv_x$ and all other advective terms in the momentum equations are set to zero, the circulation changes substantially as indicated by the linearized results shown in Figs. 7c and 7d. The downwelling below the SML is greatly reduced and all isopycnals slope up toward the shelf at depths less than 300 m. The offshore flow in the central region of wind forcing is also greatly reduced since the absolute anticyclonic high in sea level disappears (Fig. 9a). A relative high does remain near $x = (60, 1900) \text{ km}$ and a cross-shelf ridge in sea level is still present. Near the western end of the forcing region, the trough in sea level has deepened offshore.

A quantitative measure of the effect of removing the nonlinear terms is given by the net transports shown in Fig. 6b. The transport of the westward coastal jet through transect 2 is reduced by 0.5 Sv (about 50%) over that obtained when the nonlinear terms were included (Fig. 6a). This reduction leads to a similar reduction in the offshore transport through transect 5 (0.3 Sv) and associated downwelling.

Notably, the transport of 1.7 Sv through transect 3 changes little from that obtained when the nonlinear terms were retained and the offshore transport through transect 6 increases to 0.6 Sv. These results are discussed further in section 5.

b. A scaling for the nonlinear term

For the shelf topography, wind field and stratification adopted, the nonlinear advective term $\rho_0 uv_x$ is clearly important to the shelf circulation. For other oceanic regimes it may be less so, and its importance relative to the pressure gradient p_y may be readily estimated using scales from CTW theory (e.g., Clarke 1977). In particular, for the n th CTW mode, pressure may be expanded as $p = \sum \phi_n(y) F_n(x, z)$ where the F_n are eigenfunctions, $b_n = F_n(0, 0)$, and the amplitude satisfies

$$\partial \phi_n / \partial y = b_n \tau \quad (3a)$$

within the region of wind forcing, assuming steady conditions and no bottom friction. At the eastern end of the forcing region, the above yields

$$\phi_n(L_w) = b_n \tau L_w. \quad (3b)$$

With h_0 the depth at the coast, the b_n satisfy

$$\sum h_0 b_n^2 = 1 \quad (3c)$$

so that the total pressure gradient at the coast is given by

$$p_y = \tau / h_0. \quad (4)$$

To estimate $\rho_0 uv_x$, (3b), (3c), and geostrophy $fv = p_x / \rho_0$ yield

$$v_x(0, L_w) = \tau L_w / (\rho_0 f h_0 L_s^2), \quad (5)$$

where $\partial^2 F_n / \partial^2 x$ has been approximated by b_n / L_s^2 , L_s is

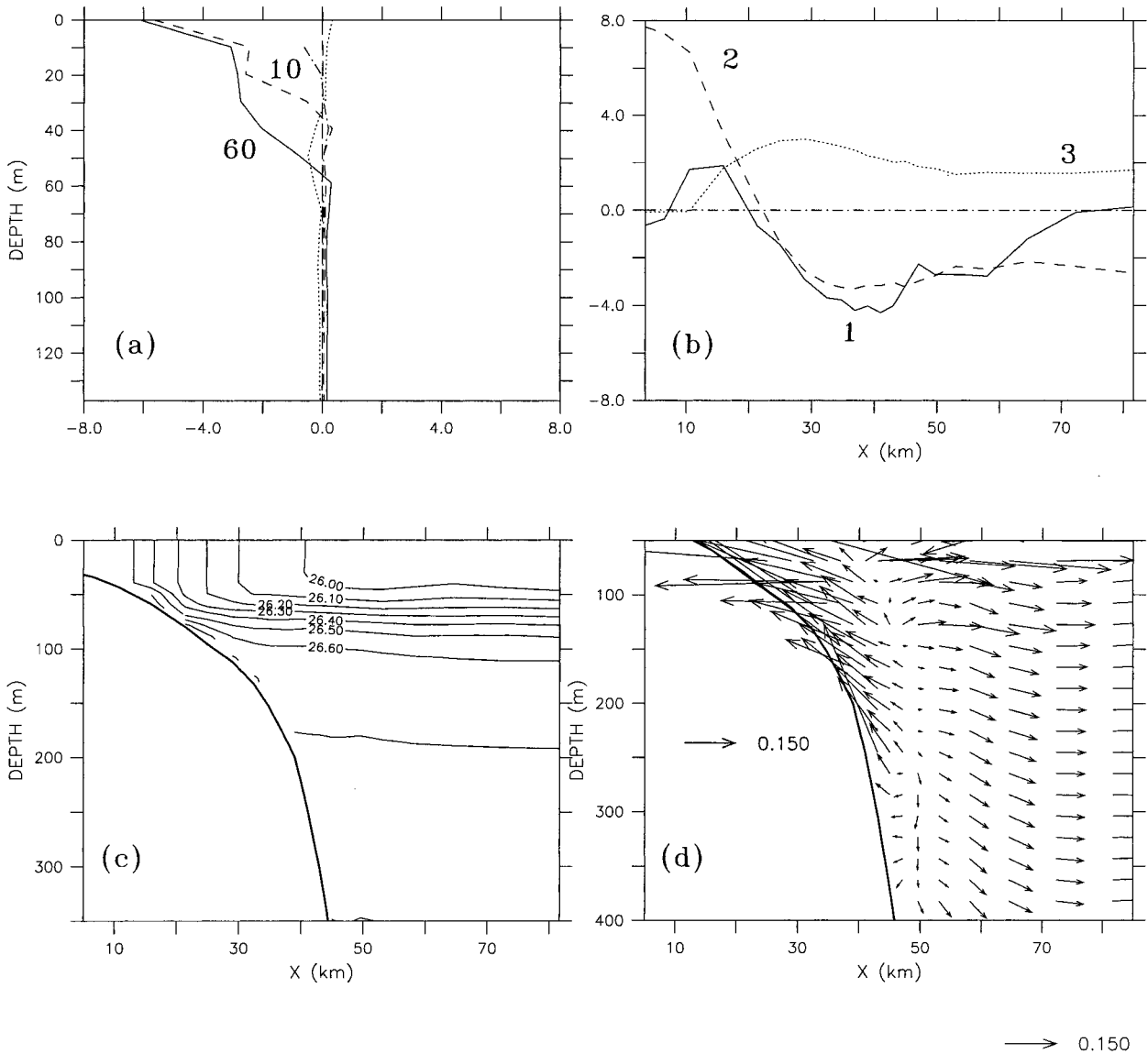


FIG. 7. Central experiment results at transect 2: (a) The nonlinear terms at $x = 45$ km: The $-\rho_0 uv_x$ term at days 10 (dashed) and 60 (solid) is labeled. The dash-dot and dotted curves correspond to $-\rho_0 vv_x$ and $-\rho_0 ww_x$ at day 60. Each term has been multiplied by 10^4 . Units $\text{kg s}^{-2} \text{m}^2$. (b) Terms in the alongshore momentum equation averaged over the mixed layer depth of 40 m. Results are presented for **1** the nonlinear term $-\rho_0 \overline{uv_x}$, **2** the sealevel term $-\rho_0 g \eta_y$ and **3** the density term $-\overline{p_y}$. Each term has been multiplied by 10^4 . Unit $\text{kg s}^{-2} \text{m}^2$. Linearized results at transect 2 and day 60: (c) The density field σ . Units kg m^{-3} , interval 0.1 kg m^{-3} . (d) The $(u, 100w)$ vector field. A vector of length 0.15 cm s^{-1} vector is indicated. Note that for clarity, results for the SML in the top 50 m have been excluded from the plot.

a scale of the shelf width (the distance from the coast to the shelf break), and the sum over all modes has been taken. Unlike p_y , v_x and the velocity $v(0, L_w)$ at the edge of the forcing region, increase with the wind fetch L_w since for CTW dynamics the total alongshore transport must balance that drawn offshore by the surface Ekman flux.

Now using (5) and the Ekman scaling $u \approx u_E = \tau/(\rho_0 f H_m)$ results in the estimate

$$\rho_0 uv_x = \tau^2 L_w / (\rho_0 h_0 H_m L_s^2 f^2), \quad (6)$$

and the ratio of nonlinear to pressure gradient terms is given by

$$I = \rho_0 uv_x / p_y = (\tau / \rho_0) L_w / (H_m L_s^2 f^2). \quad (7a)$$

Finally, to eliminate the SML depth, we adopt the scaling by Pollard et al. (1973), $H_m = (u_* / f)(f/N)^{1/2}$, where $u_* = (\tau / \rho_0)^{1/2}$ is the friction velocity and N the near-surface buoyancy frequency. The ratio I then becomes

$$I = (u_* / f)(N/f)^{1/2} L_w / L_s^2. \quad (7b)$$

The result (7b) indicates that the relative importance

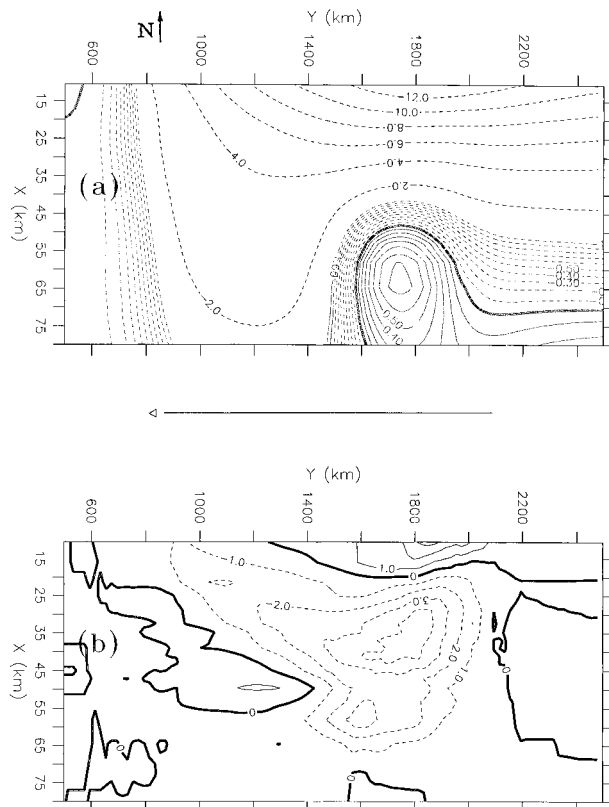


FIG. 8. Central experiment results. (a) The sea level field at day 60. The contour interval is 2 cm for $\eta \leq -1$ cm and 0.1 cm for $\eta \geq -1$ cm. Dashed contours indicate negative sealevel displacement. The direction north (N) is indicated above the panel. The region of wind forcing is indicated by the arrow above the panel. (b) The nonlinear term $-\rho_0 \overline{uv}_x$ multiplied by 10^4 . Dashed contours are negative. Units $\text{kg s}^{-2} \text{m}^2$.

of the nonlinear term increases with near-surface stratification, wind stress, wind fetch, and for narrow shelves. The increase with stratification occurs because the SML depth decreases with N so that $u \approx u_E$ must be larger. The increase with $1/L_s$ occurs because the alongshore transport is trapped closer to the coast.

The scaling and result (7b) seem plausible, although the neglect of bottom friction means that the amplitude of the pressure field obtained from (3)–(4) is overestimated. However, since both p_y and p_x are overestimated by a similar amount, the ratio I should not be unduly compromised. Moreover, the scaling (7b) is readily evaluated for the numerical results here and the nonlinear and pressure gradient terms are comparable, as found for the model output (Fig. 7b). Specifically, with $u_*/f = 10^2$, $L_w = 1200$ km, $L_s = 35$ km, and $N/f \approx 100$, the ratio is given by $I = 0.98$.

c. Alongshore gradients of density within the SML

While removal of the nonlinear terms leads to a large reduction in the magnitude of the anticyclonic eddy, a

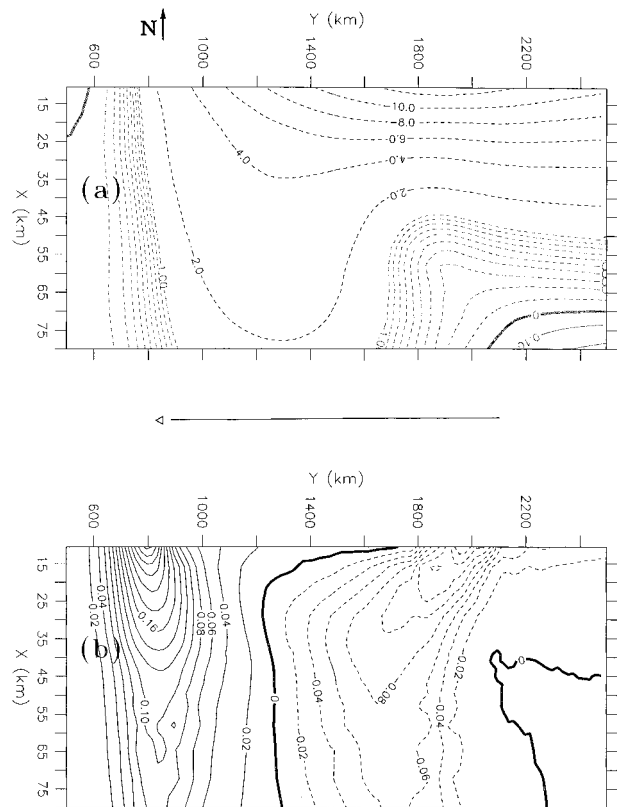


FIG. 9. Linearized experiment results at day 60. (a) The sea level field. The contour interval is 2 cm for $\eta \leq -1$ cm and 0.1 cm for $\eta \geq -1$ cm. Dashed contours indicate negative sealevel displacement. The direction north (N) is indicated above the panel. The region of wind forcing is indicated by the arrow above the panel. (b) The geostrophic velocity u_m that is associated with the alongshore gradient of density within the 40 m deep SML. Dashed contours indicate flow toward the coast. Units cm s^{-1} .

relative high remains near $x = (60, 1900)$ km and a cross-shelf ridge in sea level is still present (Fig. 9a). Near the western end of the forcing region, the trough in sea level has deepened offshore.

The most likely explanation for these residual variations in sea level lies in the geostrophic velocity associated with the alongshore gradients of density within the SML. Ignoring for the moment gradients of sea level, a cross-shelf geostrophic velocity may be defined by

$$u_m = (-1/\rho_0 f) \partial p^m / \partial y, \quad (8)$$

where $p^m = \int_{-H_m}^0 g \rho dz$ is the pressure below the SML ($-h \leq z \leq -H_m$), depth $H_m = 40$ m. The velocity extends to all depths below the SML with values over the slope of about 0.05 cm s^{-1} (Fig. 9b), which are comparable with the model results (e.g., Fig. 7d). This velocity and the alongshore density gradient are also largest near the ends of the forcing region since, outside of this region, the wind is zero and upwelling, offshore advection, and vertical mixing are negligible.

Now at the eastern end of the forcing region the geo-

strophic velocity u_m is onshore (negative) and should lead to the production of anticyclonic vorticity and ridging of sea level shown in Fig. 9a. To the west, the geostrophic velocity u_m necessarily changes sign and the offshore flow should lead to vortex stretching, the production of cyclonic vorticity, and a trough in sea level. The alongshore gradient of sea level associated with the ridge and trough should in turn act to drive a secondary geostrophic offshore flow over most of the central region, leading to a lowering of coastal sea level. This lowering and the predictions above are qualitatively consistent with the numerical results found (Fig. 9a).

This explanation is explored further in the appendix using a semianalytical model of geostrophic adjustment in the SML. The model predicts an anticyclonic gyre with cross-shelf velocities that are a factor of 5 smaller than found above. It is argued that changes in shelf depth, unaccounted for in the adjustment model, would act to amplify the magnitude of the cross-shelf velocities.

d. Heat flux results

To provide further substance to these speculations, two additional numerical experiments were made by applying surface fluxes of heat and salinity (outlined in section 2) that act to minimize density gradients within the SML. In the first experiment, the nonlinear advective terms were retained, and the surface fluxes resulted in a fivefold reduction in the alongshore density gradient DGY_x and velocity u_m (Fig. 10b). Since u_m is now much smaller, the associated alongshore gradient of sea level should also be smaller, and the secondary geostrophic offshore flow reduced. The cross-shelf trough and cyclonic eddy should thus be reduced in magnitude. A region of convergence and anticyclonic eddy are still expected since these were argued to result primarily from nonlinear advection.

These hypotheses are consistent with the numerical results for sea level shown in Fig. 10a. The cyclonic gyre and cross-shelf trough are now absent and the anticyclonic eddy extends over the entire region of wind forcing. At transect 2, the results for density and velocity are very similar to those shown in Fig. 3, and downwelling occurs from the base of the SML to depths of more than 400 m. At transect 1, the results shown in Fig. 11 are different from those obtained without surface heating. The offshore flow and downwelling over the slope are larger due to the more extensive anticyclonic eddy. The eastward undercurrent over the slope is weaker since the cross-shelf gradient of sea level is larger (due to the more extensive eddy), while the cross-shelf gradient of density within the SML is smaller (due to the surface heating).

The net transports of the current system were examined and that directed through transect 5 was found to be halved to 0.25 Sv since a sea level trough and

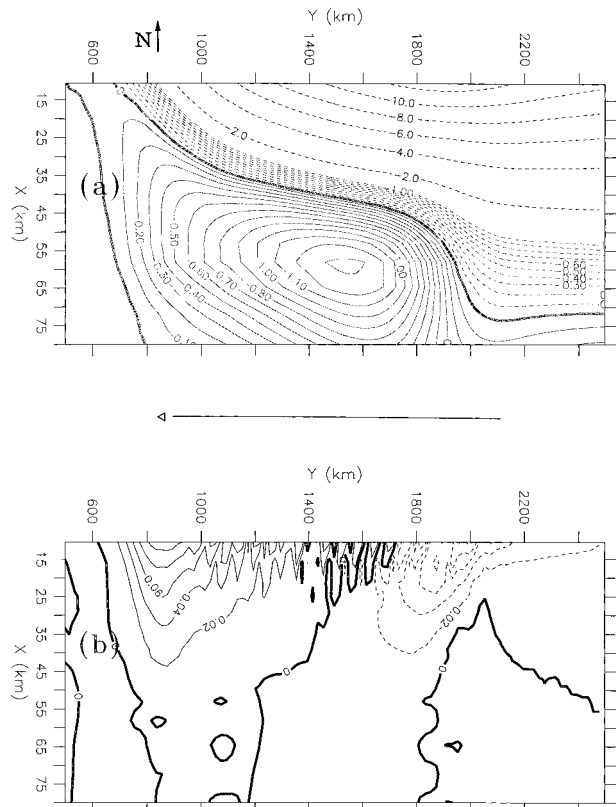


FIG. 10. Heat flux results (nonlinear) at day 60. (a) The sea level field. The contour interval is 2 cm for $\eta \leq -1$ cm and 0.1 cm for $\eta \geq -1$ cm. Dashed contours indicate negative sealevel displacement. The direction north (N) is indicated above the panel. The region of wind forcing is indicated by the arrow above the panel. (b) The geostrophic velocity u_m that is associated with the alongshore gradient of density within the 40 m deep SML. Dashed contours indicate flow toward the coast. Units cm s^{-1} .

cyclonic eddy no longer result from the alongshore gradient of density. The excess of 0.25 Sv was, instead, found to be driven to the west by the more extensive anticyclonic eddy, and the transport of the westward coastal jet through transect 1 increased to 0.7 Sv. The net transport through transect 3 remained unchanged at 1.8 Sv.

Results were also obtained with the surface fluxes of heat and salt, but without the nonlinear advective terms. That is, both mechanisms for eddy formation were minimized and the sea level results show (Fig. 12a) that the ridge and trough in sea level near the eastern and western ends of the forcing region are all but eliminated. The sea level pattern more closely resembles that which may be obtained from a linear CTW model in which SML and nonlinear effects are absent (Suginohara 1982).

The net transports were also examined and are found to be similar to those obtained when just the nonlinear terms were set to zero (Fig. 6b). The westward coastal jet transport through transects 3 and 2 were unchanged.

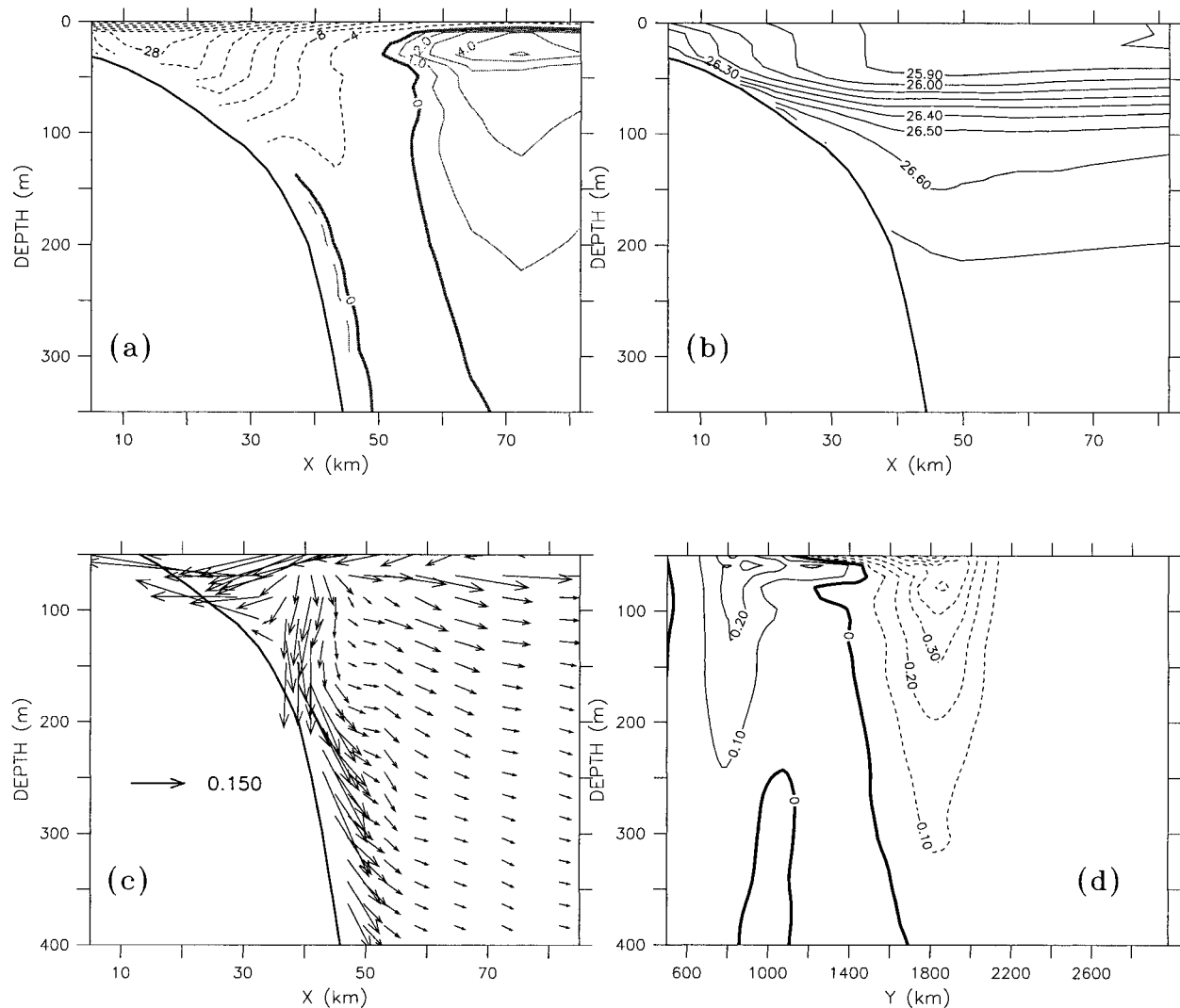


FIG. 11. Heat flux results (nonlinear) at transect 1 and day 60. (a) The alongshore velocity field v . The solid (dashed) contours indicate flow to the east (west) with an interval of 4 cm s^{-1} (1 cm s^{-1}). (b) The density field σ_t . Units kg m^{-3} , contour interval 0.1 kg m^{-3} . (c) The $(u, 100w)$ vector field. A vector of length 0.15 cm s^{-1} vector is indicated. Note that for clarity, results for the SML in the top 50 m are excluded from the plot. (d) The cross-shelf velocity u obtained 50 km from the coast at day 60. The contour interval is 0.2 cm s^{-1} . Note that for clarity, results for the SML in the top 50 m are excluded from the plot.

However, due to the near elimination of the cross-shelf ridges in sealevel, the transport of the westward coastal jet through transect 1 increased by 0.1 Sv while the offshore transports within the forcing region were half of the values shown in Fig. 6b.

e. Sensitivity to the wind stress distribution

The nonlinear advection and alongshore gradients of density are clearly important to the overall circulation within the region of wind forcing. However, as shown in Figs. 8 and 9, these terms are also largest near the edges of the forcing region where the wind stress is tapered to zero. While each of the cosine-bell tapers extend over 400 km, it may be that the effects of these

terms become unimportant as the domain of the tapers increases in size.

To test this speculation, the domain of the eastern taper was doubled from $y \in (1800, 2200) \text{ km}$ to $y \in (1600, 2400) \text{ km}$, while that at the western end remained unchanged (Fig. 12). (We have in mind that the western taper would represent an abrupt change in the orientation of the coastline.) The maximum value of the stress was again taken as 0.1 Pa so that the total offshore transport by the wind remains unchanged at 1.2 Sv . The largest difference between the two wind stress distributions (Fig. 12) amounts to 0.025 Pa or 25% of the total and, while not large, should enable the sensitivity of results to be established.

The results for sea level are shown in Fig. 12b and

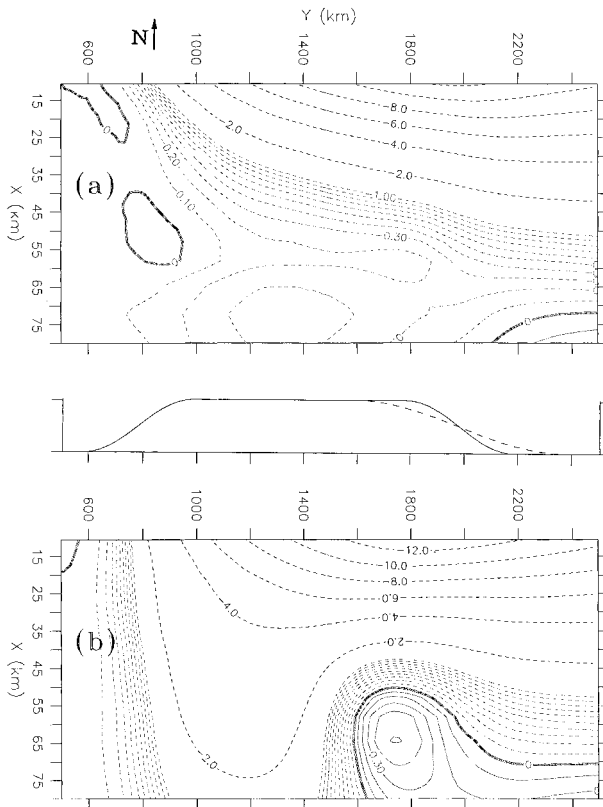


FIG. 12. Results for the sea level field at day 60. The contour interval is 2 cm for $\eta \leq -1$ cm and 0.1 cm for $\eta \geq -1$ cm. Dashed contours indicate negative sealevel displacement. The direction north (N) is indicated above the panel. The original and large-taper distributions of wind stress are indicated by the solid and dashed curves in the middle panel. (a) Heat flux results (linear). (b) Large taper results (nonlinear).

in accord with the 25% reduction in wind stress at $y = 1800$ km, the magnitude of the anticyclonic eddy (and $-\rho_0 \overline{uv}_x$) is reduced by about 20%. Otherwise, the results are qualitatively similar to those found for the central experiment (Fig. 8). The geostrophic velocity u_m was also reduced by about 20% but it, and all other results were similar to those presented above.

The effects that arise from nonlinear advection and the alongshore gradient of density are thus not overly sensitive to the distribution of wind stress, but rather appear to simply scale with the magnitude.

5. Circulation and transports in the far field

The above results demonstrate the importance of the nonlinear terms and alongshore gradients of density in determining the excess transport and distribution, within the region of wind-forcing. However, these SML effects have little impact on the net transport through section 3 since, in all of the numerical experiments above, the total was found to be about 1.8 Sv, or 0.6 Sv larger than that drawn offshore by the wind (Fig. 6). Moreover, in

all cases, the results for density, velocity, and transport were found to be very similar to those obtained for the central experiment (Fig. 13).

In the following, an explanation is sought for why the results are so similar and why the transports are larger than that removed by the wind. The likely answers to these questions involve bottom friction and we begin by examining the cross-shelf circulation and upwelling at transect 3.

a. The circulation

Consider first the central experiment results for density and the cross-shelf velocity at day 60 (Fig. 13). The 120-m elevation of the $26.6 \sigma_t$ surface is comparable to that found within the forcing region (Fig. 3d) and results from the transport within the bottom boundary layer and the frictional decay of the alongshore velocity, whereby $(hU_r)_x \approx -(hV)_y$.

As noted by Allen et al. (1995), the effects of the bottom boundary layer can also lead to downwelling. At $x = 30$ km, the onshore transport within the boundary layer [$hU_b = -\tau^b/(\rho_0 f)$] accounts for almost all of the total hU_r (Fig. 13c). The cross-shelf divergence of the boundary layer flow results in the localized downwelling near the shelf break, while above the boundary layer the onshore flow is near zero. Closer inshore, the effects of the coastal wall become evident. The total onshore flow hU_r becomes small and, above the boundary layer, an offshore flow is found.

A similar form of downwelling may occur within the forcing region since the bottom boundary layer transport contributes up to 60% of the total onshore transport hU_r , shoreward of about $x \approx 30$ km, while farther offshore, the boundary layer transport is near zero (Fig. 13d). Such downwelling, if significant, is obscured by the general downwelling that is driven by the effects of the SML.

b. The dynamics of the far field

As noted, the results for all of the numerical experiments were found to be very similar to those presented for the central experiment. To see why this is the case, we first note that there is little variation between the sea level fields obtained for each of the numerical experiments near transects 2 and 3 and within 30 km of the coast (Figs. 8a, 9a, 10a, and 12a). These nearshore fields also change little after day 10 (e.g., Fig. 3) since they are largely set up by the propagation of first mode CTWs and not by effects within the SML (e.g., Middleton and Cirano 1999). Indeed, within 40 km of the coast, the alongshore geostrophic transport $hV_s = -SGX/(\rho_0 f)$ for both the central and linear experiments changes little after day 10 and is nearly identical in each case (Fig. 14a).

Farther offshore, the transports hV_s do increase with time and for the central experiment, the total (integrated

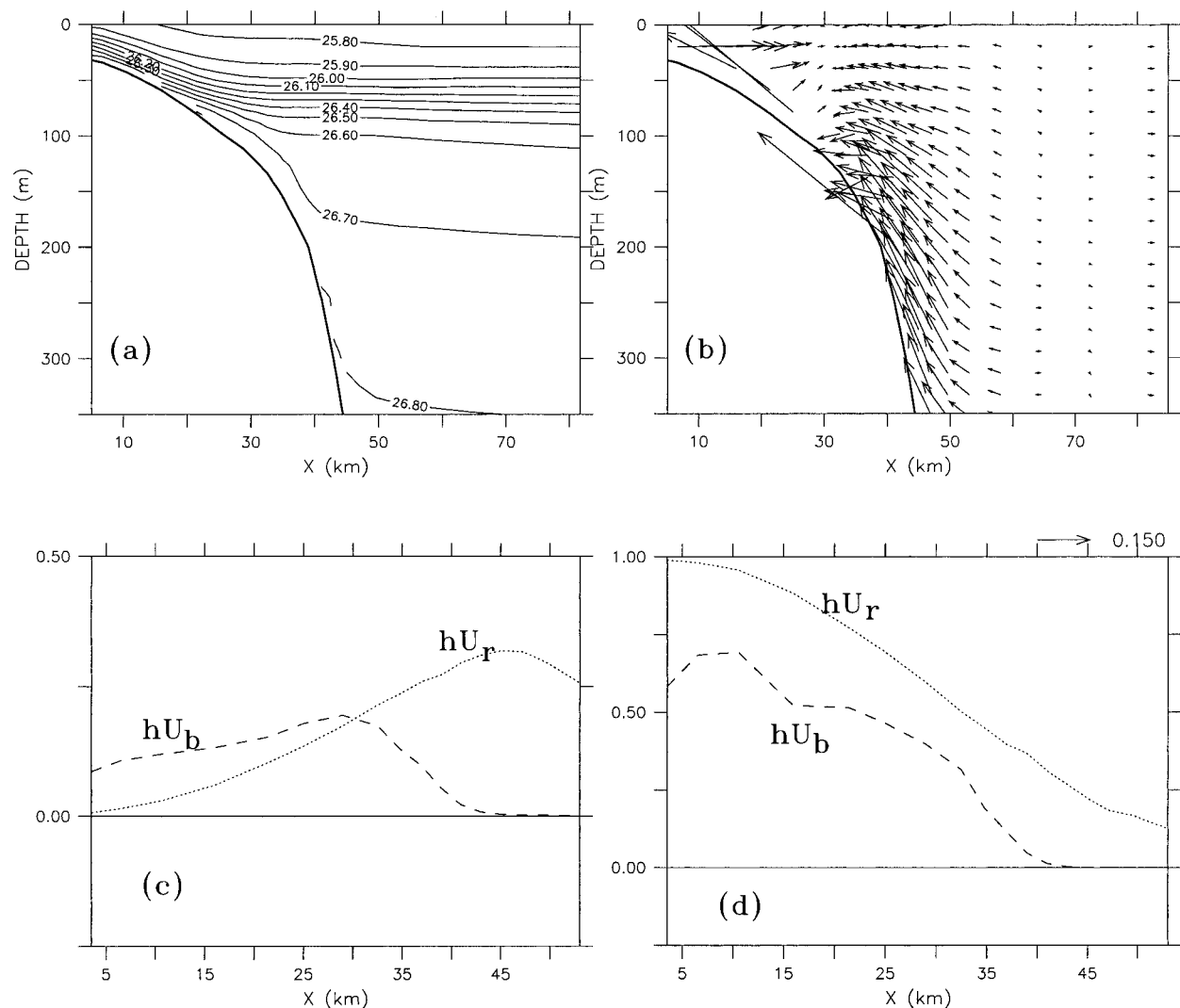


FIG. 13. Central experiment results at transect 3 and day 60. (a) The density field σ_r . Units kg m^{-3} , interval 0.1 kg m^{-3} . (b) The $(u, 100w)$ vector field. A vector of length 0.15 cm s^{-1} is indicated. (c) The cross-shelf transport $hU_b = -\tau^b/(\rho_0 f)$ within the bottom boundary layer as estimated from the bottom stress τ^b and the total cross-shelf transport hU_r . A positive value indicates transport toward the coast. Units $\text{m}^2 \text{ s}^{-1}$. (d) As in (c) but for transect 2.

out to $x = 100 \text{ km}$) increases from 2.2 Sv at day 10 to 2.8 Sv at day 60. On the other hand, the opposing transport due to the thermal-wind shear $hV_d = -DGX/(\rho_0 f)$ changes little in each case and the results for each experiment are again similar. (For clarity, only the day 60 results are presented.) The change in the depth-integrated transport hV_d is small since the upwelling and thermal-wind shear are largest inshore of the shelf break, where the water is relatively shallow, or within the thin boundary layer close to the slope (Fig. 13a).

The net result is that in each case, the sum $hV = hV_s + hV_d$ becomes larger over the slope (Fig. 14c) and for the central experiment, the total increases from 1.2 Sv to 1.8 Sv . The growth in transport in all experiments is due to changes in sea level rather than density.

The mechanism for the changes in sea level over the

slope is thought to be due to bottom friction. As noted, friction leads to an onshore transport within the bottom boundary layer and also to a divergence v_y that acts to draw water onshore within the interior. The resultant vortex squashing over the slope intensifies the alongshore velocity and transport hV_s . Since this process is driven by a velocity field that is largely set up at around day 10 by the CTWs, the results for the velocity, density, and alongshore transport are similar for each of the numerical experiments.

6. Summary and discussion

Using the Princeton Ocean Model, the problem of upwelling over a uniform shelf has been reinvestigated. The purpose of the study was to elucidate the circulation

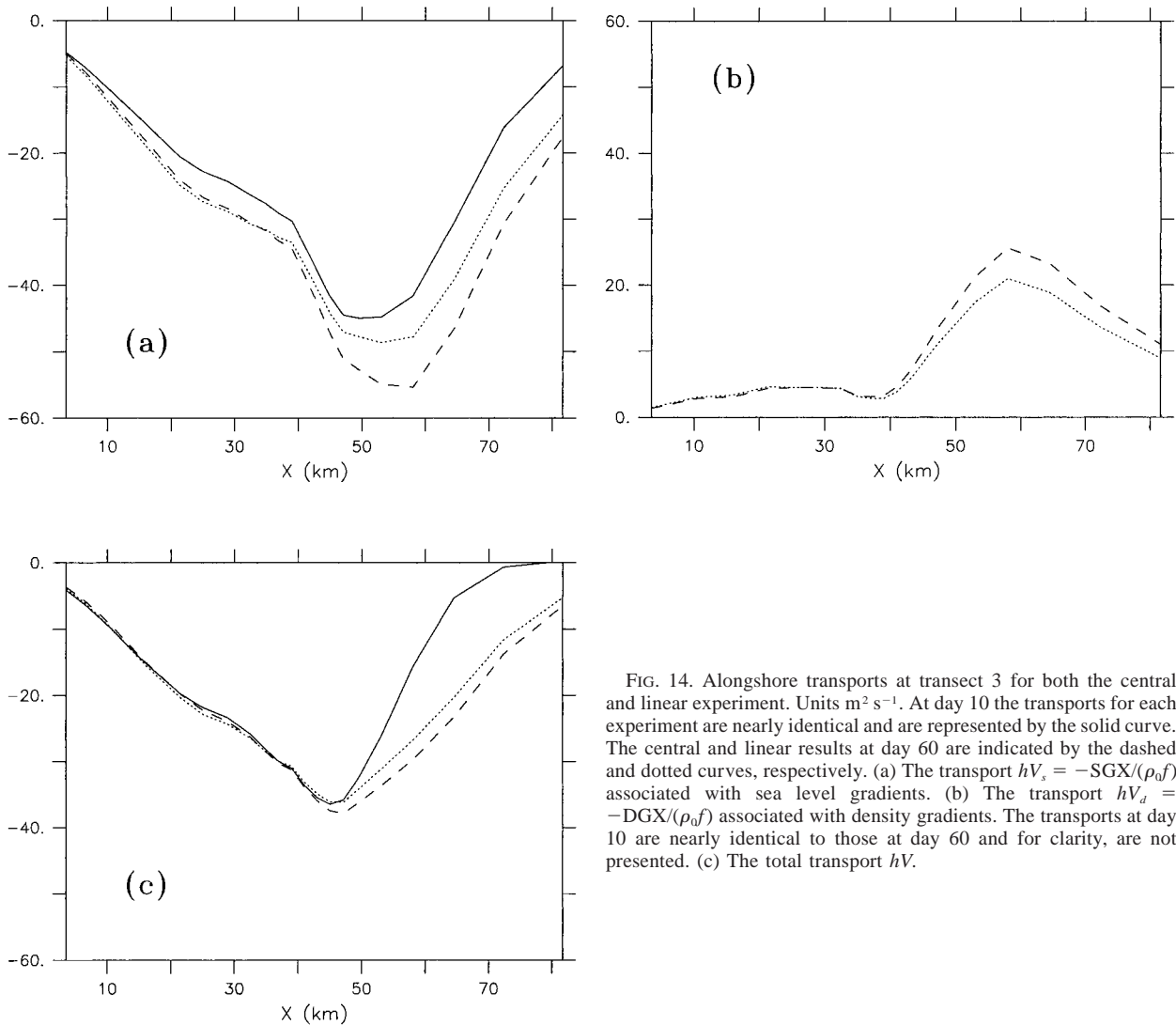


FIG. 14. Alongshore transports at transect 3 for both the central and linear experiment. Units $\text{m}^2 \text{s}^{-1}$. At day 10 the transports for each experiment are nearly identical and are represented by the solid curve. The central and linear results at day 60 are indicated by the dashed and dotted curves, respectively. (a) The transport $hV_s = -SGX/(\rho_0 f)$ associated with sea level gradients. (b) The transport $hV_d = -DGX/(\rho_0 f)$ associated with density gradients. The transports at day 10 are nearly identical to those at day 60 and for clarity, are not presented. (c) The total transport hV .

and cause of the anticyclonic eddy and associated downwelling reported originally by Sugimoto (1982) and Sugimoto and Kitamura (1984).

These authors made little comment about the anticyclonic eddy, although in the solutions here it was found to dominate the circulation over the continental slope after 30 days or so. In the central experiment (nonlinear and zero heating), the rise in sea level of the eddy after 60 days was found to be about 1 cm with nearsurface currents of up to 4 cm s^{-1} . The growth of this eddy was attributed to an excess in the alongshore transport within the forcing region. Much of this excess was expelled offshore within the central forcing region, resulting in a downwelling of isopycnals over the slope.

Sugimoto and Kitamura (1984) suggested (but did not show) that the downwelling was due to a two-cell circulation that can arise near sharp SML fronts. There is no strong evidence of such a two-cell circulation here, and the downwelling is found over and beyond the

slope. Rather, two new mechanisms for the formation of the eddies within the region of wind forcing were identified. The most important involves the cross-shelf advection of alongshore momentum within the SML, which acts to accelerate the alongshore flow leading to an excess in alongshore transport within the region of wind forcing. The second mechanism was argued to involve the alongshore gradients of density that through geostrophy, can drive cross-shelf flows leading to vortex stretching and squashing.

In the context of the former mechanism, the cross-shelf advection of alongshore momentum $\rho_0 u v_x$ was found to be the largest of all the nonlinear terms within the SML and of comparable magnitude to the pressure gradients due to sea level and density. The effect of the term is to accelerate the alongshore flow, leading to a convergence within the SML that is manifest by a rise in sea level and downwelling over the slope—the generation of the anticyclonic eddy. When this and all other

nonlinear advection terms were set to zero, the downwelling over the slope and amplitude of the anticyclonic eddy were greatly reduced.

Using scales from linear CTW theory, the importance of nonlinear advection was estimated by

$$\rho_0 uv_x/p_y = (u_*/f)(N/f)^{1/2}L_w/L_s^2.$$

The result shows that nonlinear effects will increase with wind stress and near-surface stratification, since the SML depth is smaller and u larger, and with wind fetch and decreasing shelf width, since the alongshore velocity over the shelf will be larger.

A second mechanism that modifies the slope circulation was argued to involve the cross-shelf geostrophic velocity u_m , associated with the alongshore gradients of density within the SML. The velocity u_m is largest near the eastern and western ends of the region of wind forcing and was hypothesized to lead to the onshore and offshore flow and production of anticyclonic and cyclonic vorticity found in the model solutions.

Support for this mechanism was obtained in two ways. First, numerical solutions were obtained using surface fluxes of heat and salt that act to minimize the density gradients within the SML. In these results, the cyclonic eddy largely disappeared and the anticyclonic eddy was found to extend over the entire region of wind-forcing. Second, a semianalytic model for the geostrophic adjustment of a dense "upwelled" anomaly was derived to show that such alongshore gradients in density would lead to the development of an anticyclonic gyre in a flat shallow ocean. While the cross-shelf velocities were quite weak, it was argued that these would be amplified by changes in shelf depth.

While the SML effects identified above are important to the downwelling and circulation within the region of wind forcing, the dynamics far to the east seem quite different. Results for the velocity, density, and alongshore transport were found to be very similar in each of the numerical experiments and, thus, only weakly dependent on the effects that arise from nonlinear advection and density gradients within the SML.

The similarity of results was hypothesized to arise from the following process. Over the first 10 days, the nearshore circulation in each case is similar, being largely set up by the first mode CTWs that propagate in from the forcing region. Bottom friction is thus similar in each case and the resultant onshore flow and vortex squashing leads to a similar pattern of upwelling and enhancement of the alongshore velocity over the slope. The enhanced slope velocity in turn leads to a net alongshore transport that is, by day 60, about 1.8 Sv or 50% larger than that drawn offshore by the wind.

The upwelling at transect 3 was also as large as that found within the forcing region, although confined more to the bottom boundary layer and nearshore region. Downwelling over the shelfbreak was also found and shown to be driven by the divergence of the onshore

transport within the bottom boundary layer (Allen et al. 1995).

The results obtained here, and in other two-dimensional studies highlight the variety of scales that are important to coastal upwelling. For a flat bottom, stratified ocean with no alongshore variations, the fundamental scale of upwelling is the internal deformation radius. Where a shelf topography is included, but bottom friction excluded, isopycnal displacement may be determined largely by the angle of the shelf slope (Pedlosky 1978). With the inclusion of bottom friction, the bottom boundary layer can become an important conduit of upwelled water and, as noted above, variations in shelf slope can lead to localized downwelling (Allen et al. 1995).

For three-dimensional upwelling, the scales of motion are initially determined by linear, inviscid CTWs (Suginohara 1982). As shown here however, density gradients and nonlinear advection within the SML can ultimately effect the nature of the circulation over the shelf, and the entire region of wind forcing. A parametric study of the relative importance of these mechanisms and associated scales is beyond the scope of this study but might be profitably examined in the future.

In conclusion, the principle results of this upwelling study relate to the identification of two new mechanisms within the SML that are important to the slope circulation of wind-forcing region. While the bottom topography and stratification adopted were idealized, the results were not found to be crucially dependent on the distribution of wind stress and may prove useful in the interpretation of other modeling studies and in the analysis of field data. Indeed, the scaling for the relative importance of nonlinear advection can be readily estimated for any upwelling regime. It is likely that, in the real ocean, the circulation driven by the SML effects would be subsequently overwhelmed by that due to baroclinic instability. However, it is also possible that the anticyclonic eddy that arises from the SML effects could influence the onset of baroclinic instability and that these effects could also be important to the subsequent dynamics and circulation.

Acknowledgments. This research was supported by an Australian Research Council Grant A39700800. I thank Alan Blumberg and George Mellor for making their model freely available, NOAA/PMEL for use of the FERRET graphics package, and Mauro Cirano for help in drafting some figures. Many of the numerical experiments were conducted on the Fujitsu VPP300 housed at the Supercomputer Facility, Australian National University. I also thank Chris Mooers for some constructive comments.

APPENDIX

Geostrophic Adjustment within the Surface Mixed Layer

A simple model for the geostrophic circulation driven by density gradients within the SML is considered. A

semi-infinite ocean, depth H_m , is adopted with a coastal wall at $x = 0$. The equations for the model are

$$\bar{u}_t - f\bar{v} = -g\bar{N}_x, \quad \bar{v}_t + f\bar{u} = -g\bar{N}_y, \quad (A1)$$

$$\eta_t + H_m \nabla \cdot \bar{\mathbf{u}} = 0, \quad (A2)$$

where the overbar denotes an average over the SML depth $H_m = 40$ m, $N = \eta + \eta'$, and $\eta' = \int_z^0 \rho'/\rho_0 dz$ denotes an equivalent sea level due to the upwelled density perturbation $\rho' = \rho - \rho_0$. The anomaly ρ' is assumed to be centered on $y = 0$, constant over the adjustment timescale and independent of z so that $\bar{\eta}' = \rho'H_m/(2\rho_0)$. The equation for the steady adjusted solution for \bar{N} may be obtained from (A1) and (A2) and written as

$$a^2 \nabla^2 \bar{N} - \bar{N} = -\bar{\eta}', \quad (A3)$$

where $a^2 = gH_m/f^2$ and the initial state is one of rest with $\eta = 0$. The condition of $\bar{u} = 0$ at the coast ($x = 0$) implies that $\bar{N}_y = 0$. A local solution is sought and, since we assume that $\eta' \rightarrow 0$ as $|\mathbf{x}| \rightarrow \infty$, then $\bar{N} = 0$ at $x = 0$ and as $x \rightarrow \infty$.

With these conditions, the Greens function solution to (A3) may be written as

$$\bar{N} = - \int_{-\infty}^{\infty} \int_{-\infty}^{\infty} G(\mathbf{x}, \mathbf{x}_0) \bar{\eta}'(\mathbf{x}_0) dx_0 dy_0, \quad (A4a)$$

where

$$G(\mathbf{x}, \mathbf{x}_0) = -\frac{1}{2\pi a^2} \left[K_0 \left| \frac{\mathbf{x} - \mathbf{x}_0}{a} \right| - K_0 \left| \frac{\mathbf{x} - \mathbf{x}_0^*}{a} \right| \right], \quad (A4b)$$

K_0 is the modified Bessel function, $\mathbf{x}_0 = (x_0, y_0)$ and $\mathbf{x}_0^* = (-x_0, y_0)$.

Solutions to \bar{N} and η were obtained for the idealized density anomaly

$$\rho' = Ae^{(-x/L_x)} e^{(-y^2/2L_y^2)}, \quad (A5)$$

with $L_x = 40$ km, $L_y = 200$ km, $A = 1$ kg m⁻³, $f = -10^{-4}$ s⁻¹ and $H_m = 40$ m. With these parameters, the maxima of the alongshore and cross-shelf density gradients are similar in magnitude to those found in the numerical solutions.

Now the condition at the coast is that $\bar{N} = 0$ so that at the origin, $\eta = -\bar{\eta}' = -2$ cm. More generally, the results for η shown in Fig. A1 (upper panel) closely mimic the forcing, $-\bar{\eta}'$ and the dense anomaly sits lower in the water. The total pressure field \bar{N} (Fig. A1, lower panel), is small compared to either the forcing or sea level fields. The reason for this is that the dominant term in the left side of (A3) will involve the cross-shelf scale L_x , since from the choice of parameters above,

$$\left(\frac{a}{L_x}\right)^2 \gg \left(\frac{a}{L_y}\right)^2 = 1.$$

Thus, \bar{N} will scale with

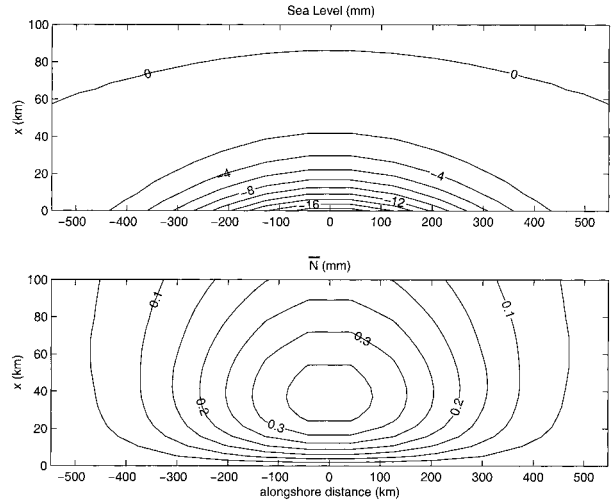


FIG. A1. Geostrophically adjusted solutions for a constant “upwelled” density anomaly. Upper panel: sea level, units mm. Lower panel: The total depth-integrated pressure field as measured by \bar{N} , units mm.

$$\left(\frac{L_x}{a}\right)^2 \bar{\eta}'$$

and be small.

An anticyclonic gyre does result with cross-shelf velocities of order 0.01 cm s⁻¹. These velocities are a factor of 5 smaller than those obtained from the Princeton Ocean Model. However, since pressure is continuous with depth, such velocities would extend to all depths over a sloping shelf and the convergence in shallower water would act to amplify the magnitude. For example, the onshore velocity at the eastern end of the forcing region might reasonably increase by a factor of 10 between the 1000-m and 100-m isobaths.

A significant change in sea level might also be expected. A scaling based on bottom slope $\eta \approx -h_x \int_0^t u_m dt$ (with $h_x = 0.004$ and $u_m = -0.05$ cm s⁻¹ for the 100-m isobath) indicates a 2-m rise in sea level over 10 days. The estimate here is admittedly crude and makes no allowance for divergence of the horizontal flow. However, it does suggest that alongshore variations in density should result in an increase (decrease) in sea level, and in the production of anticyclonic (cyclonic) vorticity.

REFERENCES

- Allen, J. S., P. A. Newberger, and J. Federiuk, 1995: Upwelling circulation on the Oregon continental shelf. Part I: Response to idealized forcing. *J. Phys. Oceanogr.*, **25**, 1843–1866.
- Blumberg, A., and G. Mellor, 1987: A description of a three dimensional coastal ocean circulation model. *Three-Dimensional Coastal Ocean Models*, N. Heaps, Ed., Amer. Geophys. Union.
- Brink, K. H., 1983: The near surface dynamics of coastal upwelling. *Progress in Oceanography*, Vol. 12, Pergamon, 223–257.
- Clarke, A. J., 1977: Observational and numerical evidence for wind-

- forced coastal-trapped long waves. *J. Phys. Oceanogr.*, **7**, 231–247.
- Haidvogel, D. B., A. Beckmann, and K. S. Hedstrom, 1991: Dynamical simulations of filaments formation and evolution in the coastal transition zone. *J. Geophys. Res.*, **96**, 15 017–15 040.
- Huyer, A., R. L. Smith, and T. Paluskiewicz, 1987: Coastal upwelling off Peru during normal and El Niño times, 1981–1984. *J. Geophys. Res.*, **92**, 14 297–14 307.
- McCreary, J. P., 1981: A linear stratified model of the coastal undercurrent. *Philos. Trans. Roy. Soc. London*, **302A**, 385–413.
- , Y. Fukamachi, and P. K. Kundu, 1991: A numerical investigation of jets and eddies near an eastern ocean boundary. *J. Geophys. Res.*, **96**, 2515–2534.
- Middleton, J. F., and M. Cirano, 1999: Wind-forced downwelling slope currents: A numerical study. *J. Phys. Oceanogr.*, **29**, 1723–1743.
- Mooers, C. N. K., C. A. Collins, and R. L. Smith 1976: The dynamical structure of the frontal zone in the coastal upwelling region off Oregon. *J. Phys. Oceanogr.*, **6**, 3–21.
- Pedlosky, J., 1978: An inertial model of steady coastal upwelling. *J. Phys. Oceanogr.*, **8**, 171–177.
- Pollard, R., P. Rhines, and R. Thompson 1973: The deepening of the wind-mixed layer. *Geophys. Fluid Dyn.*, **3**, 381–404.
- Schahinger, R., 1987: Structure of coastal upwelling events observed off the south-east coast of South Australia. *Aust. J. Mar. Freshwater Res.*, **38**, 439–459.
- Smith, R. L., 1994: The physical processes of coastal ocean upwelling systems. *Upwelling in the Ocean*, C. P. Summerhayes, K.-C. Emeis, and B. Zeitzschel, Eds., Environ. Sci. Rep. ES 18, Wiley and Sons, 39–64.
- Suginohara, N., 1977: Upwelling front and two-cell circulation. *J. Oceanogr. Soc. Japan*, **33**, 115–130.
- , 1982: Coastal upwelling: Onshore–offshore circulation, equatorward coastal jet, and poleward undercurrent over a continental shelf–slope. *J. Phys. Oceanogr.*, **12**, 272–284.
- , and Y. Kitamura, 1984: Long term coastal upwelling over a continental shelf–slope. *J. Phys. Oceanogr.*, **14**, 1095–1104.
- Wang, D.-P., 1982: Development of a three-dimensional limited-area (island) shelf circulation model. *J. Phys. Oceanogr.*, **12**, 605–616.